



This is a repository copy of *Synthesis, characterisation and preliminary corrosion behaviour assessment of simulant Fukushima nuclear accident fuel debris*.

White Rose Research Online URL for this paper:
<http://eprints.whiterose.ac.uk/158896/>

Version: Accepted Version

Article:

Gausse, C. orcid.org/0000-0002-7392-7507, Dunlop, C.W., Friskney, A.A. et al. (3 more authors) (2020) Synthesis, characterisation and preliminary corrosion behaviour assessment of simulant Fukushima nuclear accident fuel debris. *MRS Advances*, 5 (1-2). pp. 65-72. ISSN 2059-8521

<https://doi.org/10.1557/adv.2020.35>

This article has been published in a revised form in *MRS Advances* <http://doi.org/10.1557/adv.2020.35>. This version is free to view and download for private research and study only. Not for re-distribution, re-sale or use in derivative works. © 2020 Materials Research Society.

Reuse

This article is distributed under the terms of the Creative Commons Attribution-NonCommercial-NoDerivs (CC BY-NC-ND) licence. This licence only allows you to download this work and share it with others as long as you credit the authors, but you can't change the article in any way or use it commercially. More information and the full terms of the licence here: <https://creativecommons.org/licenses/>

Takedown

If you consider content in White Rose Research Online to be in breach of UK law, please notify us by emailing eprints@whiterose.ac.uk including the URL of the record and the reason for the withdrawal request.



eprints@whiterose.ac.uk
<https://eprints.whiterose.ac.uk/>

Synthesis, characterisation and preliminary corrosion behaviour assessment of simulants Fukushima nuclear accident fuel debris

Clémence Gausse, Calum W. Dunlop, Aidan A. Friskney, Martin C. Stennett, Neil C. Hyatt and Claire L. Corkhill

NucleUS Immobilisation Science Laboratory, Department of Materials Science and Engineering, The University of Sheffield, United Kingdom

ABSTRACT

Nuclear fuel debris generated at the Fukushima Daiichi nuclear power plant during the loss of coolant accident in 2011, still resides within the reactor units, constantly cooled by water. Until it is retrieved, the fuel debris will corrode, releasing radioactive elements into the coolant water and the ground surrounding the reactors. To predict the corrosion behaviour of these materials, and to establish parameters for experiments with U-containing and real fuel debris, the corrosion of two surrogate fuel debris materials, with a composition of $Ce_{(1-x)}Zr_xO_2$ ($x = 0.2$ and 0.4), was investigated. Materials were synthesised by a wet chemistry route and pellets were sintered at 1700°C in air atmosphere. Due to the slow corrosion kinetics, aggressive conditions were applied, and corrosion experiments were performed in 9 mol.L^{-1} HNO_3 under static conditions. The incorporation of Zr into the structure of Ce reduced the normalised dissolution rate; from $(3.75 \pm 0.15) \times 10^{-6}\text{ g.m}^{-2}.\text{d}^{-1}$ to $(4.96 \pm 0.28) \times 10^{-6}\text{ g.m}^{-2}.\text{d}^{-1}$ for $R_L(\text{Ce})$ of $Ce_{0.8}Zr_{0.2}O_2$ and $Ce_{0.6}Zr_{0.4}O_2$, respectively.

INTRODUCTION

The earthquake and tsunami that occurred on the 11th March 2011 at the Fukushima Daiichi Nuclear Power Plant (NPP) resulted in a loss of coolant accident and the partial meltdown of boiling water reactor Units 1 to 3 [1–3]. The temperature in the reactors rose in excess of 2000°C causing the melting and the reaction of UO_2 pellets with the steam-oxidised zircaloy fuel cladding. The resulting material, known as Nuclear Fuel Debris (NFD), is principally a $\text{U}_{1-x}\text{Zr}_x\text{O}_2$ solid solution containing a variety of fission products and minor actinides, including a significant proportion of Pu from MOX fuel [4,5]. According to historic nuclear accidents, it is also suggested that the formation of

glassy or ceramic admixtures of fuel, cladding and reactor components, known as Molten Core – Concrete Interaction Products (MCCIs), occurred at Fukushima. Continuous water injection (firstly seawater, followed by groundwater from the area surrounding the Fukushima NPP and then filtered water) has been used since the accident to cool the NFD and MCCIs, and reduced the temperature below 100°C [2]. In this so-called stable cold shutdown situation, analysis of coolant water effluent evidenced the presence of Pu, indicating the fuel debris is being dissolved. The aqueous leaching of fuel debris is expected to alter its chemical and mechanical properties, especially at the interface with the coolant water. It may also result in the formation of secondary alteration products, which should be considered a significant respirable hazard for retrieval and decommissioning[1,3,4,6].

Since it is not possible to enter the reactor due to the high radiation hazard, and because robots are currently not sufficiently radiation-resistant to remain within the reactor to obtain samples of NFD, it is necessary to use low activity analogues to study the behaviour of these materials. We here present the results of a study of the synthesis and corrosion of an inactive surrogate for NFD, using Ce as an analogue for Pu, in two $Ce_{(1-x)}Zr_xO_2$ solid solutions.

MATERIALS AND METHODS

Synthesis

The following reactants were used as starting materials: $ZrOCl_2 \cdot 8H_2O$, $CeCl_3$ and NH_4OH . All the reagents used were of analytical-grade and supplied by Sigma-Aldrich. Pure CeO_2 and $Ce_{(1-x)}Zr_xO_2$ ($x = 0.8$ and 0.6) were synthesised by mixing a solution of $ZrOCl_2$ and $CeCl_3$ in the desired molar quantities. The hydroxide precursor is obtained by adding NH_4OH solution (5 mol L^{-1}) until the pH reaches 9. The precipitate was centrifuged and washed with deionised water to remove Cl^- , and with isopropanol and subsequently dried at 60°C. The hydroxide precursor was calcined at 750°C for 4h under reducing atmosphere ($N_2/5\% H_2$).

The calcined powder was milled and pressed using a uniaxial press into a 6mm diameter pellet. The sintering of the samples was performed through conventional sintering at 1700°C, for 8 hours in air.

Characterisation

The crystalline phase assemblage was determined by powder X-ray diffraction (XRD) using a Bruker D2 Phaser X-ray diffractometer in reflectance mode. The apparatus is equipped with $Cu K\alpha_{1,2}$ radiation ($\lambda = 1.5418 \text{ \AA}$). Data were recorded at room temperature in the angular range of $20^\circ < 2\theta < 100^\circ$, with a step size $\Delta(2\theta) = 0.02^\circ$ and a total counting time of about 30 minutes per sample.

The morphology of the samples was imaged using a Hitachi TM3030 scanning electron microscope (SEM) with semi-quantitative analysis using a built-in Bruker XFlash 430H energy dispersive X-ray spectroscopy (EDS) system.

Prior to leaching experiments, the density of CeO_2 and the $Ce_{(1-x)}Zr_xO_2$ solid solutions were obtained by geometric density measurements and by Archimedes balance analysis. The density was determined by comparing the apparent density (g cm^{-3} –

determined by geometric measurements) with the theoretical density of the solid solutions (determined from XRD unit cells refinement). The total closed porosity was obtained by Archimedes balance analysis. From these measurements, the open porosity was calculated.

The grain size was determined from SEM images analysis of 50 to 300 grains, using Fiji software [7]. The specific surface area was determined using the SESAM method (Study of Evolving Surface Area by Microscopy) developed in the ICSM Laboratory, detailed in full in [8]. Briefly, SEM micrographs were recorded at low magnification and binarised by Fiji software to determine the surface area of the visible pores. The pore size distribution of the analysed domain was assumed to be representative of the whole sample. It was further assumed that the pores were cylindrical. The surface area of the pores was determined from the proportion of open porosity. The specific surface area was then calculated using the resulting surface area and the mass of the sample.

Corrosion behaviour

Due to the highly refractory nature of $Ce_{(1-x)}Zr_xO_2$, the corrosion behaviour was evaluated on a short time scale, in concentrated HNO_3 (9 mol.L⁻¹). The dissolution experiments were performed in closed Polytetrafluoroethylene (PTFE) containers under static conditions. The pellets were put in contact with 30 mL of HNO_3 . The dissolution vessels were placed in a controlled temperature oven (60°C). Before each sampling, the dissolution vessels were manually stirred to homogenise the solution. Aliquots of 1.2 mL were taken for analysis and renewed by fresh dissolution media at regular intervals time to maintain a constant total volume throughout the experiment. In these conditions, less than 3 % of the leachate was renewed for each uptake, which avoided perturbations of the solid/liquid system during the establishment of saturation processes. Aliquots were then filtered using a 0.22 µm filter to eliminate colloids.

Elemental concentrations were determined by ICP-MS (Inductively Coupled Plasma Mass Spectroscopy – ThermoFisher RQ) after dilution in 0.16 mol.L⁻¹ HNO_3 . The protocol used allowed the detection of Zr and Ce with a detection limit of 10 and 100 ppt, respectively, and a relative error of 5 %. The evolution of the dissolution reaction was followed through the normalised mass loss $N_L(i,t)$ (g.m⁻²), defined as:

$$N_L(i,t) = \frac{m_i(t)}{f_i \times S} \quad (1)$$

where $m_i(t)$ (g) is the mass of element i measured in solution at time t , S (m²) is the reactive surface area of the solid in contact with the solution and f_i (g g⁻¹) is the mass ratio of the element i in the solid. The reactive surface area of the sample is:

$$S = S_{SA} \times m_0 \quad (2)$$

where S_{SA} (m² g⁻¹) denotes the initial surface area of the solid determined by SESAM method, and m_0 (g) is the initial mass of the solid introduced in the system. The mass of element i released in the dissolution medium is then determined through the measurement of its elementary concentration, C_i (M), following:

$$C_i = \frac{c_i \times V}{M_i} \quad (3)$$

where V (L) is the volume of the dissolution medium in contact with the solid and M_i ($\text{g}\cdot\text{mol}^{-1}$) is the molecular mass of the element i . The normalized dissolution rate, $R_L(i)$ ($\text{g}\cdot\text{m}^{-2}\cdot\text{d}^{-1}$), is defined as the time-derivative of the normalized mass loss, i.e. :

$$R_L(i) = \frac{dN_L(i)}{dt} = \frac{1}{f_i \times S} \times \frac{dm_i}{dt} \quad (4)$$

The use of Equation (4) can be considered acceptable as long as the reactive surface area remains almost constant. This assumption was supported by the strong refractory character of CeO_2 and ZrO_2 [9,10], and by the associated very low dissolution rates determined in the following sections. For a congruent dissolution, the $R_L(i)$ values determined from the release in solution of each constitutive element are equal to the dissolution rate of the solid.

RESULTS AND DISCUSSION

Characterisation of CeO_2 and $\text{Ce}_{1-x}\text{Zr}_x\text{O}_2$ ($x = 0.2$ and 0.4)

The X-ray Diffraction patterns of CeO_2 and $\text{Ce}_{1-x}\text{Zr}_x\text{O}_2$ are presented in Figure 1. A single phase material was obtained in all samples, with the fluorite structure type (cubic $Fm\bar{3}m$ space group), characteristic of CeO_2 . The patterns were refined by the Rietveld method using TOPAS software. A shift was observed in the main reflections of the fluorite lattice to higher 2θ angles when Zr was incorporated, due to a reduction in the lattice parameter induced by the substitution of Zr (ionic radius of 0.84 \AA) for Ce (0.97 \AA).

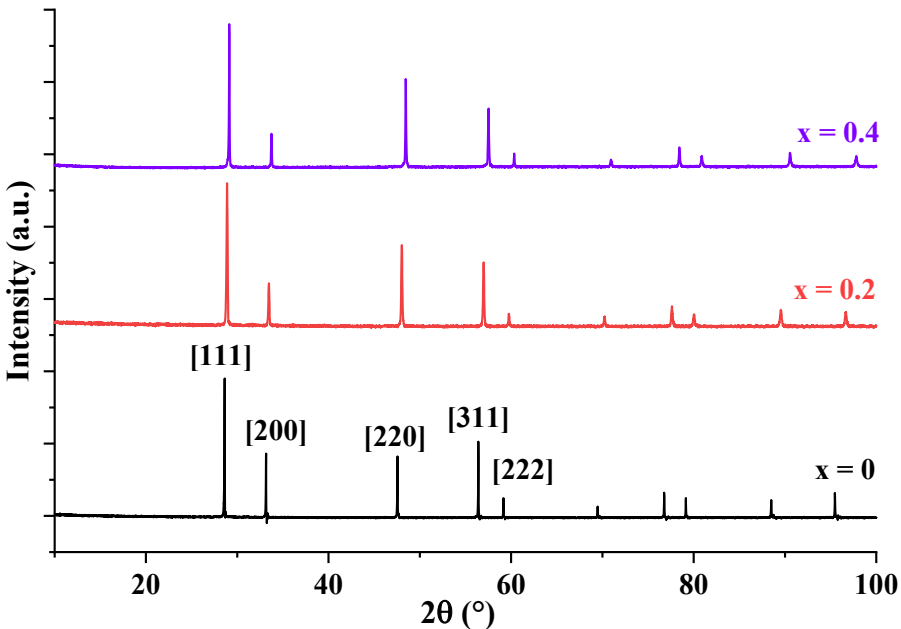


Figure 1. XRD patterns of CeO_2 (black), $\text{Ce}_{0.8}\text{Zr}_{0.2}\text{O}_2$ (red) and $\text{Ce}_{0.6}\text{Zr}_{0.4}\text{O}_2$ (purple).

The decrease in the lattice parameter became more pronounced as more Zr was incorporated into the solid solution. It decreased from $a = 5.404 \pm 0.002 \text{ \AA}$ in CeO_2 to $a = 5.308 \pm 0.001 \text{ \AA}$ in $\text{Ce}_{0.6}\text{Zr}_{0.4}\text{O}_2$.

Scanning Electronic Microscopy (SEM) observations were performed as shown in Figure 2. The three compositions had a well-defined granular structure with minor porosity. In agreement with the XRD patterns, there was no evidence of a second phase.

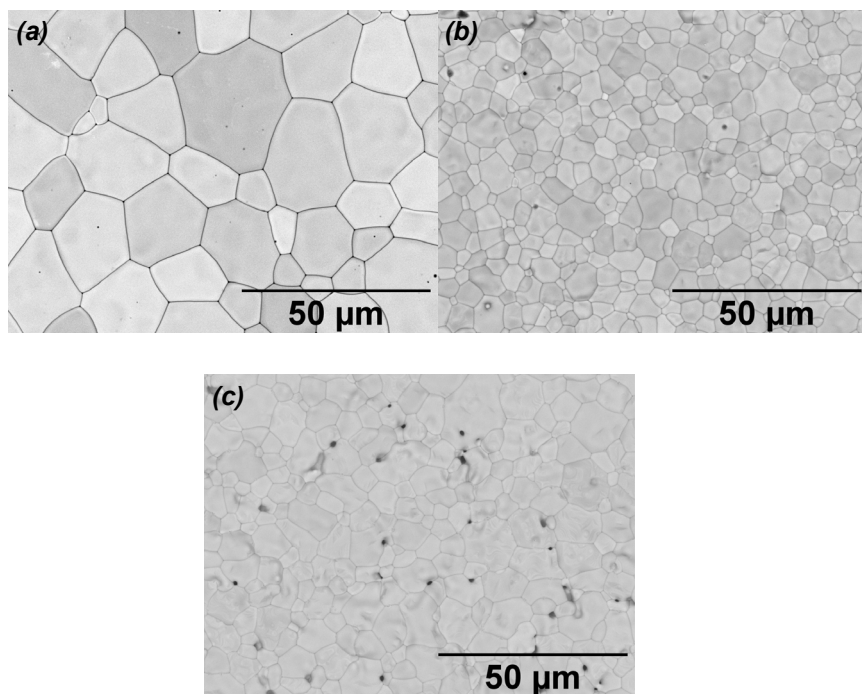


Figure 2. SEM observations of CeO_2 (a), $\text{Ce}_{0.8}\text{Zr}_{0.2}\text{O}_2$ (b) and $\text{Ce}_{0.6}\text{Zr}_{0.4}\text{O}_2$ (c).

With the incorporation of Zr, a decrease of the grain size was observed; from $14.56 \pm 0.93 \text{ μm}$ for CeO_2 to $8.94 \pm 0.97 \text{ μm}$ for $\text{Ce}_{0.6}\text{Zr}_{0.4}\text{O}_2$. The density of the three materials is shown in Table 1. As expected, the density decreased with increasing Zr content. This trend occurs as ZrO_2 is less dense than CeO_2 . However, a decrease of the open porosity and an increase of the porosity was observed when Zr was added. The open porosity decreased from $2.8 \pm 0.5 \%$ for CeO_2 to $0.7 \pm 0.5 \%$ for $\text{Ce}_{0.6}\text{Zr}_{0.4}\text{O}_2$ and the closed porosity increased from $3.7 \pm 0.5 \%$ for CeO_2 to $9.1 \pm 0.5 \%$ for $\text{Ce}_{0.6}\text{Zr}_{0.4}\text{O}_2$.

Table 1. The main characteristics of the sintered samples of CeO_2 , $\text{Ce}_{0.8}\text{Zr}_{0.2}\text{O}_2$ and $\text{Ce}_{0.6}\text{Zr}_{0.4}\text{O}_2$.

Composition	Mass (g)	Geometric density (g.cm^{-3})	Archimedes balance density (g.cm^{-3})	Theoretical density (g.cm^{-3})	Total density (%)	Open porosity (%)	Closed porosity (%)	Specific surface area ($\text{m}^2.\text{g}^{-1}$)
CeO_2	0.484	6.77 ± 0.38	6.98 ± 0.05	7.243	93.5 ± 0.5	2.8 ± 0.5	3.7 ± 0.5	$(3.05 \pm 0.58) \times 10^{-4}$
$\text{Ce}_{0.8}\text{Zr}_{0.2}\text{O}_2$	0.487	6.59 ± 0.42	6.59 ± 0.02	7.049	93.5 ± 0.5	0.02 ± 0.05	6.5 ± 0.5	$(3.15 \pm 0.10) \times 10^{-4}$

$Ce_{0.6}Zr_{0.4}O_2$	0.487	6.14 ± 0.53	6.18 ± 0.03	6.799	90.2 ± 0.5	0.7 ± 0.5	9.1 ± 0.5	$(3.37 \pm 0.52) \times 10^{-4}$
-----------------------	-------	-----------------	-----------------	-------	----------------	---------------	---------------	----------------------------------

Dissolution of CeO_2 and $Ce_{1-x}Zr_xO_2$ ($x = 0.2$ and 0.4)

The normalised mass loss of $Ce_{0.6}Zr_{0.4}O_2$ and $Ce_{0.8}Zr_{0.2}O_2$ in $9 \text{ mol.L}^{-1} \text{ HNO}_3$ at 60°C was calculated using Eqn. (1); the results, in addition to the percentage of the pellet dissolved, are shown in Figure 3.

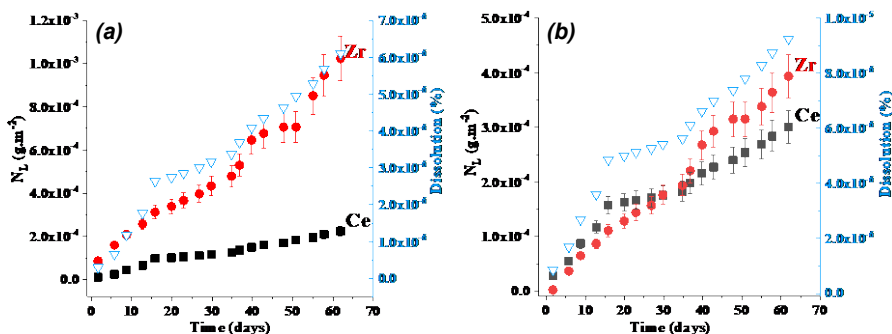


Figure 3. Evolution of the Normalised mass loss (Zr: ● and Ce: ■) and percentage dissolved (▽) of $Ce_{1-x}Zr_xO_2$ (a) $Ce_{0.8}Zr_{0.2}O_2$; and (b) $Ce_{0.6}Zr_{0.4}O_2$, in $9 \text{ mol.L}^{-1} \text{ HNO}_3$ at 60°C .

The normalised mass loss of Ce and Zr in the 20 mol.% composition were slightly higher than that of the 40 mol.% sample. For example, at 61 days, $N_L(\text{Zr})$ was $(1.02 \pm 0.15) \times 10^{-3} \text{ g.m}^{-2}$ and $N_L(\text{Ce})$ was around $(2.24 \pm 0.34) \times 10^{-4} \text{ g.m}^{-2}$ for $Ce_{0.8}Zr_{0.2}O_2$, compared to $(3.00 \pm 0.45) \times 10^{-4} \text{ g.m}^{-2}$ and $(3.94 \pm 0.59) \times 10^{-4} \text{ g.m}^{-2}$ for $N_L(\text{Zr})$ and $N_L(\text{Ce})$ of $Ce_{0.6}Zr_{0.4}O_2$, respectively. As the dissolved mass losses are very low ($< 10^{-5} \%$), we have considered all of the data to calculate the normalised dissolution rate, $R_{L,i}(t)$, by linear regression (Fig. 3), as well as the congruence ratio $r = R_L(\text{Ce})/R_L(\text{Zr})$; these are summarised in Table 2.

Table 2. Normalised dissolution rates of $Ce_{0.8}Zr_{0.2}O_2$ and $Ce_{0.6}Zr_{0.4}O_2$ in HNO_3 9M at 60°C .

Composition	$R_L(\text{Ce})$ ($\text{g.m}^{-2}.\text{d}^{-1}$)	$R_L(\text{Zr})$ ($\text{g.m}^{-2}.\text{d}^{-1}$)	r
$Ce_{0.6}Zr_{0.4}O_2$	$(4.96 \pm 0.28) \times 10^{-6}$	$(6.15 \pm 0.16) \times 10^{-6}$	0.81 ± 0.11
$Ce_{0.8}Zr_{0.2}O_2$	$(3.75 \pm 0.12) \times 10^{-6}$	$(1.35 \pm 0.04) \times 10^{-5}$	0.28 ± 0.13

The normalised dissolution rates of the $Ce_{0.8}Zr_{0.2}O_2$ sample was higher than the $Ce_{0.6}Zr_{0.4}O_2$ sample. The normalised dissolution rates of Ce and Zr, under these conditions, were congruent for the $Ce_{0.6}Zr_{0.4}O_2$ sample, as the congruence ratio is between 1/3 and 3 [11]. The dissolution rate for the $Ce_{0.8}Zr_{0.2}O_2$ sample was not congruent, as the ratio of the Ce/Zr dissolution was only 0.28.

To understand the effect that Zr incorporation is having on the dissolution rate it is important to compare the results of this study to those of pure CeO_2 . The calculated dissolution rate associated with the kinetically controlled dissolution of CeO_2 at 90°C in $0.01 \text{ mol.L}^{-1} \text{ HNO}_3$ was reported to be $(1.76 \pm 0.4) \times 10^{-5} \text{ g.m}^{-2}.\text{d}^{-1}$ [12]. This value is higher than the dissolution rate of $Ce_{0.6}Zr_{0.4}O_2$ of $(3.75 \pm 0.12) \times 10^{-6} \text{ g.m}^{-2}.\text{d}^{-1}$, which

suggests that the incorporation of Zr into the structure of Ce reduced the rate of dissolution significantly, as the conditions experienced by the samples in this project were much more extreme, 9 mol.L⁻¹ compared to 0.01 mol.L⁻¹.

CONCLUSION

Non-active analogues for nuclear fuel debris have been investigated, with the ultimate aim of supporting the future decommissioning of Fukushima Daiichi Nuclear Power Plant. Two different compositions of Ce/Zr solid solution, Ce_(1-x)Zr_xO₂ (x =0.2 and 0.4) were synthesised. These materials present a fluorite structure type, characteristic of the UO₂, making them a good structural analogue for nuclear fuel debris. A decrease in grain size and pellet density was observed with larger amount of Zr incorporated.

The dissolution behaviour was studied under 9 mol.L⁻¹ HNO₃ to gain an understanding of the corrosion behaviour. The results of this demonstrated that the presence of Zr substantially reduced the release of Ce into the solution, as compared to CeO₂, a behaviour also seen in (U,Zr)O₂ dissolution [13]. The dissolution of Zr and Ce was found to be congruent at higher Zr contents but non-congruent at lower ones. Further investigation into the leaching of these materials would allow a longer study to take place, including solutions more representative of the conditions within the Fukushima reactors. Further work is currently underway with (U,Zr)O₂ materials.

ACKNOWLEDGEMENTS

We wish to acknowledge funding for this research from the Engineering and Physical Science Research Council, under the UK-Japan Civil Nuclear grant, CHIMP (EP/R01924X/1). CLC wishes to thank EPSRC for the award of an Early Career Fellowship under grant agreement EP/N017870/1 and AAF wishes to acknowledge the Sheffield Engineering Leadership Academy (SELA) for support. This research was performed at the MIDAS Facility, at the University of Sheffield, which was established with support from the UK Department of Energy and Climate Change.

References

- [1] Nuclear Damage Compensation and Decommissioning Facilitation Corporation, Technical Strategic Plan 2017 for Decommissioning of the Fukushima Daiichi Nuclear Power Station of Tokyo Electric Power Company Holdings, Inc., 2017.
- [2] Japan Nuclear Emergency Response Headquarters, Additional Report of the Japanese Government to the IAEA - The Accident at TEPCO's Fukushima Nuclear Power Stations- (Second Report) (Summary),
http://www.kantei.go.jp/foreign/kan/topics/201106/iaea_houkokusho_e.html. (2011) 45.
<http://ci.nii.ac.jp/naid/10031060829/en/> (accessed September 4, 2019).
- [3] K. Yanagisawa, F. Imamura, T. Sakakiyama, T. Annaka, T. Takeda, N. Shuto, Tsunami assessment for risk management at nuclear power facilities in Japan, in: Pure Appl. Geophys.,

Birkhäuser-Verlag, 2007: pp. 565–576. doi:10.1007/s00024-006-0176-1.

- [4] W. Dienst, P. Hofmann, D.K. Kerwin-Peck, Chemical Interactions Between UO₂ and Zircaloy-4 from 1000 to 2000°C, *Nucl. Technol.* 65 (1984) 109–124. doi:10.13182/NT84-A33378.
- [5] T.J. Bartel, R. Dingreville, D. Littlewood, V. Tikare, M. Bertolus, V. Blanc, V. Bouineau, G. Carlot, C. Desgranges, B. Dorado, J.C. Dumas, M. Freyss, P. Garcia, J.M. Gatt, C. Gueneau, J. Julien, S. Maillard, G. Martin, R. Masson, B. Michel, J.P. Piron, C. Sabathier, R. Skorek, C. Toffolon, C. Valot, L. Van Brutzel, T.M. Besmann, A. Chernatynskiy, K. Clarno, S.B. Gorti, B. Radhakrishnan, R. Devanathan, M. Dumont, P. Maugis, A. El-Azab, F.C. Iglesias, B.J. Lewis, M. Krack, Y. Yun, M. Kurata, K. Kurosaki, R. Largenton, R.A. Lebensohn, L. Malerba, J.Y. Oh, S.R. Phillpot, J.S. Tulenko, J. Rachid, M. Stan, B. Sundman, M.R. Tonks, R. Williamson, P. Van Uffelen, M.J. Welland, C. Valot, M. Stan, S. Massara, R. Tarsi, State-of-the-Art Report on Multi-scale Modelling of Nuclear Fuels, (2015).
https://inis.iaea.org/search/search.aspx?orig_q=RN:47032405 (accessed September 4, 2019).
- [6] P. Hofmann, D. Kerwin-Peck, UO₂/Zircaloy-4 chemical interactions from 1000 to 1700°C under isothermal and transient temperature conditions, *J. Nucl. Mater.* 124 (1984) 80–105. doi:10.1016/0022-3115(84)90013-8.
- [7] T. Ferreira, W.R.- ImageJ/Fiji, undefined 2012, ImageJ user guide, Researchgate.Net. (n.d.).
<https://www.researchgate.net/file.PostFileLoader.html?id=536d58bcd039b1f84c8b45c6&assetKey=AS%3A273531969966088%40144226512749> (accessed September 5, 2019).
- [8] T. Cordara, S. Szenknect, L. Claparede, R. Podor, A. Mesbah, C. Lavalette, N. Dacheux, Kinetics of dissolution of UO₂ in nitric acid solutions: A multiparametric study of the non-catalysed reaction, *J. Nucl. Mater.* 496 (2017) 251–264. doi:10.1016/J.JNUCMAT.2017.09.038.
- [9] R.R. Prajapati, T.G. Srinivasan, V. Chandramouli, S.S. Bhagwat, Dissolution kinetics of zirconium dioxide in nitric acid, *Desalin. Water Treat.* 52 (2014) 490–497. doi:10.1080/19443994.2013.808804.
- [10] L. Claparede, N. Clavier, N. Dacheux, P. Moisy, R. Podor, J. Ravaux, Influence of Crystallization State and Microstructure on the Chemical Durability of Cerium–Neodymium Mixed Oxides, *Inorg. Chem.* 50 (2011) 9059–9072. doi:10.1021/ic201269c.
- [11] N. Vigier, S. Grandjean, B. Arab-Chapelet, F. Abraham, Reaction mechanisms of the thermal conversion of Pu(IV) oxalate into plutonium oxide, *J. Alloys Compd.* 444–445 (2007) 594–597. doi:10.1016/J.JALLCOM.2007.01.057.
- [12] C.L. Corkhill, M.C. Stennett, N.C. Hyatt, Solution Composition Effects on the Dissolution of a CeO₂ analogue for UO₂ and ThO₂ nuclear fuels, *MRS Proc.* 1744 (2015) 185–190. doi:10.1557/opl.2015.334.
- [13] Y. Kumagai, M. Takano, M. Watanabe, Reaction of hydrogen peroxide with uranium zirconium oxide solid solution – Zirconium hinders oxidative uranium dissolution, *J. Nucl. Mater.* 497 (2017) 54–59. doi:10.1016/j.jnucmat.2017.10.050.